

Nevanlinna.jl: A Julia implementation of Nevanlinna analytic continuation

Kosuke Nogaki^{1*}, Jiani Fei^{2,3}, Emanuel Gull³ and Hiroshi Shinaoka^{4,5},

¹ Department of Physics, Kyoto University, Kyoto 606-8502, Japan

² Department of Physics, Stanford University, Stanford, CA 94305, USA

³ Department of Physics, University of Michigan, Ann Arbor, MI 48104, USA

⁴ Department of Physics, Saitama University, Saitama 338-8570, Japan

⁵ JST, PRESTO, 4-1-8 Honcho, Kawaguchi, Saitama 332-0012, Japan

* nogaki.kosuke.83v@st.kyoto-u.ac.jp

February 22, 2023

Abstract

We introduce a Julia implementation of the recently proposed Nevanlinna analytic continuation method. The method is based on Nevanlinna interpolants and, by construction, preserves the causality of a response function. For theoretical calculations without statistical noise, this continuation method is a powerful tool to extract real-frequency information from numerical input data on the Matsubara axis. This method has been applied to first-principles calculations of correlated materials. This paper presents its efficient and full-featured open-source implementation of the method including the Hamburger moment problem and smoothing.

Contents

1	Introduction	2
2	Theory	3
2.1	Analytic continuation from Matsubara frequency to real frequency	3
2.2	Nevanlinna analytic continuation procedure	4
2.2.1	Definition and notations	4
2.2.2	Green functions as Nevanlinna functions	5
2.2.3	Pick criterion	5
2.2.4	Schur algorithm	6
2.2.5	Smoothing	8
2.3	Hamburger moment problem	8
3	Usage	11
3.1	Installation	11
3.2	Interface	11
3.3	Example: two-peak model	12
4	Conclusion	13

A Structure of code	16
A.1 Processing flow	16
A.2 Data struct	18
A.3 Solver struct	18
References	18

1 Introduction

In finite-temperature quantum field theories ranging from condensed matter to high energy physics, many sophisticated numerical techniques have been developed. For instance, perturbative theories [1–7] are a powerful tool for studying impurity effects [8], Fermi liquids [9, 10], and symmetry breaking phenomena such as charge-, spin-density waves [11–13], or superconductivity [14, 15]. For investigating Mott transitions and renormalization effects of quasiparticles near the Fermi energy, or Kondo effects, we may employ the non-perturbative dynamical mean-field theory [16] with discrete- [17] or continuous-time [18–21] quantum Monte Carlo impurity solvers. In the field of high-energy physics, lattice quantum chromodynamics algorithms are used for *ab initio* investigations of the masses of hadrons, the quark confinement, or of chiral symmetry breaking [22–24].

These theories are formulated in “imaginary time”, where finite-temperature statistical mechanics computations are tractable. The result of the computation is the numerical data of the Matsubara Green function $\mathcal{G}(i\omega_n)$ defined on the imaginary axis of the complex frequency plane. The spectral function $\rho(\omega) = -(1/\pi)\text{Im}G^R(\omega)$ contains information about the single-particle excitation which, in electronic systems, are related to measurements in photoemission spectroscopy. An analytic continuation step relating the Matsubara Green function $\mathcal{G}(i\omega_n)$ to the retarded Green function $G^R(\omega)$ is therefore needed as a post-processing step. This need for numerical analytic continuation exists not only for fermionic systems but also for bosonic systems [25, 26] including He [27, 28], supersolids [29], and warm dense matter [30]. Thus, a highly precise and efficient numerical analytic continuation method is desired for quantitative studies of quantum many-body systems.

Regardless of its practical importance, the numerical analytic continuation of the Green function is an ill-conditioned problem whose direct solution is intractable. To address this issue, many approximate methods have been developed. Examples include continued fraction Padé approximation methods [31], the maximum entropy method [32, 33], the stochastic analytic continuation [34–38], machine learning approaches [39], genetic algorithms [28], the sparse modeling method [40, 41], the Prony method [42], and a pole fitting approach [43]. Most of these methods are based on a regularized fit and fail to restore sharp structures in the large- ω region even for numerically exact input data. The Padé approximation, which is an interpolation method, does not ensure causality and often results in negative values of the spectral function and a violation of the sum rule, particularly at high frequencies.

The Nevanlinna analytic continuation method [44] is an interpolation method that respects the mathematical structure of causal response functions by construction, thereby producing a mathematically rigorous numerical analytic continuation that ensures causality. The formalism has been extended to matrix-valued Green functions [44, 45].

While the mathematical foundation of the Nevanlinna analytic continuation method is elegant, the numerical solution of the Nevanlinna continuation equations requires special care. The continued fraction expressions used in the method are sensitive to numerical precision, which means that the interpolation must be performed using at least quadruple floating-point arithmetic, even if input data is only known to double precision. In addition, selecting a subset of the input data such that it respects the so-called Pick condition, which guarantees causality [44], is essential to avoid overfitting. For a solvable non-degenerate problem, Nevanlinna theory guarantees the existence of an infinite number of valid analytical continuations. In practical applications, a single “best” one of these needs to be chosen, typically by imposing an additional smoothness constraint.

The sample C++ code published by the authors of [44] as a supplement to the original paper serves to illustrate Nevanlinna continuation but does not implement this smoothing step or a selection algorithm for choosing a subset of causal data. In this paper, we describe a full-featured implementation of the Nevanlinna analytic continuation method in the Julia language. Our implementation includes interpolation in arbitrary-precision arithmetic, which allows a stable interpolation. We perform the smoothing based on a numerical optimization using the automatic differentiation of the cost function, which is fast and more accurate than the numerical finite difference method. The code is straightforward to install and comes with Jupyter notebooks illustrating typical use cases. The implementation in the Julia language makes the code easily customizable for future extensions, e.g., to matrix-valued Green functions [45]. We expect that providing the user community with a ready-to-use and simple package that implements these additional steps will accelerate the adoption of the Nevanlinna method in finite temperature Green function calculations.

2 Theory

In Nevanlinna analytic continuation, the analytic properties of Green function play an essential role. We therefore describe the analytic structure of the Matsubara Green function and the retarded Green function focusing on the Lehmann representation in Sec. 2.1. In Sec. 2.2, the definition of Nevanlinna functions is given. Green functions as Nevanlinna functions, the Pick criterion, and the Schur interpolation algorithm are summarized, and the Hardy optimization procedure is explained with some technical remarks. The fundamental principles of the Hamburger moment problem are presented in Sec. 2.3. For the purpose of constructing a solution, the Hankel matrix and two distinct types of polynomials are introduced. The theory outlined here follows Ref. [44–46]. Additional technical and theoretical details explained in this paper may be useful for users of the code.

2.1 Analytic continuation from Matsubara frequency to real frequency

In this paper, we consider correlation functions between fermionic annihilation and creation operator, \hat{c} and \hat{c}^\dagger , which we call Green function. The Matsubara Green function and retarded Green function are defined as

$$\mathcal{G}(\tau) = -\langle T_\tau \hat{c}(\tau) \hat{c}^\dagger(0) \rangle, \quad (1)$$

$$G^R(t) = -i\theta(t) \langle \{\hat{c}(t), \hat{c}^\dagger(0)\} \rangle, \quad (2)$$

in the imaginary-time domain and in the real-time domain, respectively. Their Fourier-transformed functions are given by

$$\mathcal{G}(i\omega_n) = \int_0^\beta d\tau e^{i\omega_n\tau} \mathcal{G}(\tau), \quad (3)$$

$$G^R(\omega) = \lim_{\eta \rightarrow +0} \int_{-\infty}^{\infty} dt e^{i\omega t - \eta t} G^R(t) \quad (\eta > 0), \quad (4)$$

where $\langle \dots \rangle = \text{tr}\{e^{-\beta(\hat{H} - \mu\hat{N})} \dots\} / \Xi$, $\hat{c}(\tau) = e^{(\hat{H} - \mu\hat{N})\tau} \hat{c} e^{-(\hat{H} - \mu\hat{N})\tau}$, and $\hat{c}(t) = e^{i(\hat{H} - \mu\hat{N})t} \hat{c} e^{-i(\hat{H} - \mu\hat{N})t}$ with Hamiltonian \hat{H} , particle number operator \hat{N} , the inverse temperature $\beta = 1/T$, and the chemical potential μ . We take $k_B = 1$. Here, $\Xi = \text{tr}\{e^{-\beta(\hat{H} - \mu\hat{N})}\}$ is the partition function and $i\omega_n = i(2n + 1)\pi T$ are fermionic Matsubara frequencies [47]. These two Green functions are related by the Lehmann representation [48–51],

$$G(z) = \int_{-\infty}^{\infty} d\omega \frac{\rho(\omega)}{z - \omega}. \quad (5)$$

Namely, the Matsubara Green function $\mathcal{G}(i\omega_n)$ is given by the limit $z \rightarrow i\omega_n$, and the retarded Green function $G^R(\omega)$ is given by the limit $z \rightarrow \omega + i\eta$ ($\eta \rightarrow +0$). Here, the spectral function $\rho(\omega)$ is

$$\rho(\omega) = \frac{1}{\Xi} \sum_{n,m} e^{-\beta(E_n - \mu N_n)} (1 + e^{-\beta\omega}) |\langle n | \hat{c} | m \rangle|^2 \delta(\omega - E_m + E_n + \mu), \quad (6)$$

where E_n and N_n are energy and particle number of eigen state $|n\rangle$. From this definition, the positivity $\rho(\omega) \geq 0$ and the sum rule

$$\int \rho(\omega) d\omega = \frac{1}{\Xi} \sum_{n,m} (e^{-\beta(E_n - \mu N_n)} + e^{-\beta(E_m - \mu N_m)}) \langle n | \hat{c} | m \rangle \langle m | \hat{c}^\dagger | n \rangle \quad (7)$$

$$= \langle \{\hat{c}, \hat{c}^\dagger\} \rangle = 1, \quad (8)$$

follow straightforwardly. Using the formula

$$\lim_{\eta \rightarrow +0} \int \frac{f(x)}{x + i\eta} dx = \text{P} \int \frac{f(x)}{x} dx - i\pi f(0), \quad (9)$$

the spectral function can be evaluated from retarded Green function,

$$\rho(\omega) = \lim_{\eta \rightarrow +0} -\frac{1}{\pi} \text{Im} G^R(\omega + i\eta). \quad (10)$$

The central objective in this paper is to estimate $G^R(\omega + \eta)$ and $\rho(\omega)$ from the data of $\mathcal{G}(i\omega_n)$, namely, *numerical analytic continuation* between $G^R(\omega + \eta)$ and $\mathcal{G}(i\omega_n)$.

2.2 Nevanlinna analytic continuation procedure

2.2.1 Definition and notations

First, let us summarize the notations used in this paper. The upper half plane \mathcal{C}^+ and the open unit disk \mathcal{D} are

$$\mathcal{C}^+ = \{z \in \mathbb{C} | \text{Im} z > 0\}, \quad (11)$$

$$\mathcal{D} = \{w \in \mathbb{C} | |w| < 1\}. \quad (12)$$

Their closures are denoted by $\overline{\mathcal{C}^+}$ and $\overline{\mathcal{D}}$, respectively. Nevanlinna functions are holomorphic functions from \mathcal{C}^+ to $\overline{\mathcal{C}^+}$, and Schur functions are holomorphic functions from \mathcal{D} to $\overline{\mathcal{D}}$. We denote the set of Nevanlinna functions and that of Schur functions as \mathcal{N} and \mathcal{S} , respectively. Note that there is one-to-one correspondence between $z \in \mathcal{C}^+$ and $w \in \mathcal{D}$ by Möbius transformation h_ξ and the inverse h_ξ^{-1} for $\xi \in \mathcal{C}^+$:

$$w = h_\xi(z) = \frac{z - \xi}{z - \xi^*}, \quad (13)$$

$$z = h_\xi^{-1}(w) = \frac{w\xi^* - \xi}{w - 1}. \quad (14)$$

Another Möbius transformation maps $w \in \mathcal{D}$ onto $w' \in \mathcal{D}$ for $\zeta \in \mathcal{D}$:

$$w' = g_\zeta(w) = \frac{w + \zeta}{1 + \zeta^* w}, \quad (15)$$

$$w = g_\zeta^{-1}(w') = \frac{w' - \zeta}{1 - \zeta^* w'}. \quad (16)$$

2.2.2 Green functions as Nevanlinna functions

As discovered in Ref. [44, 45], the negative of fermionic Green function is a Nevanlinna function. Indeed, from Eq. (5),

$$\begin{aligned} G(x + iy) &= \int_{-\infty}^{\infty} d\omega \frac{\rho(\omega)}{x + iy - \omega} \\ &= \int_{-\infty}^{\infty} d\omega \frac{\rho(\omega)(x - \omega - iy)}{(x - \omega)^2 + y^2}. \end{aligned} \quad (17)$$

Since $\rho(\omega) \geq 0$,

$$-\text{Im} G(x + iy) = \int_{-\infty}^{\infty} d\omega \frac{\rho(\omega)y}{(x - \omega)^2 + y^2} \geq 0, \quad (18)$$

where proves $-G(z) \in \mathcal{N}$. In a numerical study, we can know the values of Green function on only finite numbers of Matsubara frequencies, $-G(Y_\alpha) = C_\alpha$ ($\alpha = 1, 2, \dots, M$). The problem is to find Nevanlinna functions $f \in \mathcal{N}$ which satisfy $f(Y_\alpha) = C_\alpha$. This problem can be modified into another tractable problem by transforming the range of Nevanlinna function by Möbius transformation. Therefore, our problem is to find a composite function $\theta = h_i \circ f : \mathcal{C}^+ \rightarrow \overline{\mathcal{D}}$ which satisfy $h_i \circ f(Y_\alpha) = h_i(C_\alpha) = \lambda_\alpha$. We call these modified Nevanlinna functions contractive functions. As discussed below, interpolation problems of contractive functions can be solved efficiently by the Schur algorithm [52, 53].

2.2.3 Pick criterion

There is a necessary and sufficient condition for the existence of Nevanlinna interpolants, namely, the generalized Pick criterion [44]. It is formulated in terms of the Pick matrix [54],

$$\left[\frac{1 - \lambda_\alpha \lambda_\beta^*}{1 - h_i(Y_\alpha) h_i(Y_\beta)^*} \right]_{\alpha, \beta} \quad \alpha, \beta = 1, 2, \dots, M. \quad (19)$$

and states that if the Pick matrix is positive definite, an infinite number of solutions to the interpolation problem exists. If it is positive semidefinite but not positive definite, there is a unique solution. If the Pick matrix contains negative eigenvalues in addition to the positive ones, no solution to the interpolation problem exists [54, 55]. In many numerical calculations, this condition is satisfied for a subset of the values to be interpolated but broken if all values are considered. In particular, if data points are added from low to high frequencies, high Matsubara frequency values tend to break this condition. Our implementation determines the optimal number of low Matsubara frequencies, N_{opt} , for the analytic continuation in an automated fashion. The process involves setting an initial value of N_{cut} to 1 and constructing a Pick matrix from input data at the lowest N_{cut} Matsubara frequencies ($\alpha = 1, \dots, N_{\text{cut}}$), which is then factorized using Cholesky Factorization. If the factorization is successful, N_{cut} is incremented by 1 and the procedure is repeated until a factorization failure occurs. The optimal cutoff, N_{opt} , is then established as the highest value of N_{cut} that resulted in a successful factorization. In the subsequent analytic continuation, we utilize only the data up to N_{opt} . We refer to this procedure as ‘‘Pick Selection’’.

2.2.4 Schur algorithm

The numerical analytic continuation can be viewed as a problem of constructing an analytic function with M point constraint conditions. That is, we aim to construct a contractive function which satisfies

$$\theta(Y_\alpha) = \lambda_\alpha \quad (\alpha = 1, 2, \dots, M). \quad (20)$$

The Schur Algorithm iteratively interpolates and constructs $\theta(z)$. In the following, we start with constructing a contractive function with one constraint, which will later be generalized to M point constraint conditions.

First, let us consider a Schur function $\varphi \in \mathcal{S}$ with one constraint condition $\varphi(0) = \gamma_1 \in \mathcal{D}$. We construct the function

$$\tilde{\varphi}(w) = \frac{1}{w} \frac{\varphi(w) - \gamma_1}{1 - \gamma_1^* \varphi(w)} \quad (21)$$

$$= \frac{1}{w} g_{\gamma_1}^{-1}(\varphi(w)). \quad (22)$$

From $g_{\gamma_1}^{-1}(\varphi(0)) = 0$ and the Schwartz’s lemma, $\tilde{\varphi}(w)$ belongs to \mathcal{S} . Conversely for any Schur function $\tilde{\varphi}(w)$,

$$\varphi(w) = \frac{w\tilde{\varphi}(w) + \gamma_1}{1 + \gamma_1^* w\tilde{\varphi}(w)} \quad (23)$$

$$= g_{\gamma_1}(w\tilde{\varphi}(w)) \quad (24)$$

will be regular in \mathcal{D} , $|\varphi(w)| < 1$, and $\varphi(0) = \gamma_1$. Therefore, Eq. (23) gives a general form of Schur functions with one constraint condition $\varphi(0) = \gamma_1$, where $\tilde{\varphi}(w)$ is an arbitrary Schur function.

Combining Eq. (23) and Möbius transformation $h_{Y_1}(z)$, a general form of contractive functions $\theta(z) = \varphi \circ h_{Y_1}(z)$ that satisfy $\theta(Y_1) = \gamma_1$ can be given as

$$\theta(z) = \frac{\frac{z - Y_1}{z - Y_1^*} \tilde{\theta}(z) + \gamma_1}{\gamma_1^* \frac{z - Y_1}{z - Y_1^*} \tilde{\theta}(z) + 1}, \quad (25)$$

where $\tilde{\theta}(z)$ is an arbitrary contractive function.

The procedure can be further expanded to problems with M constraint conditions:

$$\theta_1(Y_\alpha) = \lambda_\alpha^{(1)}. \quad (\alpha = 1, 2, \dots, M) \quad (26)$$

By utilizing Eq. (25), we can recast the M constraint problem for θ_1 as an $(M - 1)$ constraint problem for θ_2 :

$$\theta_1(z) = \frac{\frac{z-Y_1}{z-Y_1^*} \theta_2(z) + \lambda_1^{(1)}}{(\lambda_1^{(1)})^* \frac{z-Y_1}{z-Y_1^*} \theta_2(z) + 1}, \quad (27)$$

with

$$\theta_2(Y_\alpha) = \frac{Y_\alpha - Y_1^*}{Y_\alpha - Y_1} \frac{\lambda_1^{(1)} - \lambda_\alpha^{(1)}}{(\lambda_1^{(1)})^* \lambda_\alpha^{(1)} - 1} \equiv \lambda_\alpha^{(2)} \quad (\alpha = 2, 3, \dots, M). \quad (28)$$

In a similar manner, this algorithm can be continued iteratively until $\theta_1, \theta_2, \dots, \theta_M, \theta_{M+1}$ are determined, leaving θ_{M+1} as an arbitrary contractive function. The continued contractive function, which is parameterized by θ_{M+1} , can be expressed as

$$\theta(z)[\theta_{M+1}(z)] = \frac{a(z)\theta_{M+1}(z) + b(z)}{c(z)\theta_{M+1}(z) + d(z)}, \quad (29)$$

where $a(z)$, $b(z)$, $c(z)$, and $d(z)$ are determined by

$$\begin{aligned} \begin{pmatrix} a(z) & b(z) \\ c(z) & d(z) \end{pmatrix} &= \prod_{\alpha=1}^M \begin{pmatrix} \frac{z-Y_\alpha}{z-Y_\alpha^*} & \phi_\alpha \\ \phi_\alpha^* \frac{z-Y_\alpha}{z-Y_\alpha^*} & 1 \end{pmatrix} \\ &= \begin{pmatrix} \frac{z-Y_1}{z-Y_1^*} & \phi_1 \\ \phi_1^* \frac{z-Y_1}{z-Y_1^*} & 1 \end{pmatrix} \begin{pmatrix} \frac{z-Y_2}{z-Y_2^*} & \phi_2 \\ \phi_2^* \frac{z-Y_2}{z-Y_2^*} & 1 \end{pmatrix} \dots \begin{pmatrix} \frac{z-Y_M}{z-Y_M^*} & \phi_M \\ \phi_M^* \frac{z-Y_M}{z-Y_M^*} & 1 \end{pmatrix}. \end{aligned} \quad (30)$$

Here, ϕ_α ($\alpha = 1, 2, \dots, M$) is defined by $\phi_\alpha \equiv \theta_\alpha(Y_\alpha) = \lambda_\alpha^{(\alpha)}$. The retarded Green function $G^R(\omega + i\eta)$ is given by $-h_i^{-1}(\theta(\omega + i\eta))$

To determine ϕ_α , we prepare recursive algorithm. First, $\phi_1 = \theta(Y_1)$ and construct

$$\begin{pmatrix} a_2 & b_2 \\ c_2 & d_2 \end{pmatrix} = \begin{pmatrix} \frac{Y_2 - Y_1}{Y_2 - Y_1^*} & \phi_1 \\ \phi_1^* \frac{Y_2 - Y_1}{Y_2 - Y_1^*} & 1 \end{pmatrix}, \quad (31)$$

and determine ϕ_2

$$\phi_2 = \frac{-d_2 \theta(Y_2) + b_2}{c_2 \theta(Y_2) - a_2}. \quad (32)$$

In general, the values of $\phi_1, \dots, \phi_{\beta-1}$ can be utilized to determine ϕ_β as follows:

$$\begin{pmatrix} a_\beta & b_\beta \\ c_\beta & d_\beta \end{pmatrix} = \prod_{\alpha=1}^{\beta-1} \begin{pmatrix} \frac{Y_\beta - Y_\alpha}{Y_\beta - Y_\alpha^*} & \phi_\alpha \\ \phi_\alpha^* \frac{Y_\beta - Y_\alpha}{Y_\beta - Y_\alpha^*} & 1 \end{pmatrix}, \quad (33)$$

$$\phi_\beta = \frac{-d_\beta \theta(Y_\beta) + b_\beta}{c_\beta \theta(Y_\beta) - a_\beta}. \quad (34)$$

Note that these algorithms require at least quadruple floating-point precision to achieve accurate continued fraction expressions, as numerical instability may arise. This is demonstrated in Section 3.3.

2.2.5 Smoothing

There is an infinite number of “valid” continuations consistent with causal input data, since any Schur function θ_{M+1} will yield a valid spectral function. To select the “most physical” of all possible spectral functions, additional constraints for θ_{M+1} or for the final spectral function can be imposed. As discussed below, artificial oscillations around exact values appear for $\theta_{M+1}(z) = 0$. To eliminate these oscillations and get the *best* continued result, we adjust $\theta_{M+1}(z)$ in order to get the smoothest possible spectral function [44]. We assume that $\theta_{M+1}(z)$ exists in Hardy space $H^2(C^+)$ in which a function $F(z)$ satisfies [56]

$$\sup_{y>0} \int_{-\infty}^{\infty} |F(x + iy)|^2 dx < \infty. \quad (35)$$

This space is generated by the orthogonal basis $\{f^k(z)\}_0^\infty$ whose basis functions are given by

$$f^k(z) = \frac{1}{\sqrt{\pi}(z+i)} \left(\frac{z-i}{z+i} \right)^k. \quad (36)$$

We expand $\theta_{M+1}(z)$ into the basis with a cutoff parameter H_{cut} ,

$$\theta_{M+1}(z) = \sum_{k=0}^{H_{\text{cut}}} a_k f^k(z) + b_k [f^k(z)]^*, \quad (37)$$

and minimize the cost function

$$F[\theta_{M+1}] = \left| 1 - \int_{-\infty}^{\infty} \rho(\omega) d\omega \right|^2 + \lambda \int_{-\infty}^{\infty} (\rho''(\omega))^2 d\omega. \quad (38)$$

Typically, a value of $\lambda = 10^{-4}$ has been observed to result in stable solutions. In `Nevanlinna.jl`, we use automatic differentiation to optimize coefficients a_k, b_k . The implementation is based on `Zygote.jl` [57] and `Optim.jl` [58]. The automatic differentiation is extraordinarily efficient and accurate up to machine precision, unlike the numerical finite difference method employed in Ref. [44].

In practical calculations, a large H_{cut} can lead to numerical instabilities. As such, our methodology adopts a *step-by-step* approach. Once convergence has been achieved for a solution (a_k, b_k) at some H_{cut} , we initiate optimization of the cost function for $H_{\text{cut}} + 1$ by utilizing the previous convergence values $(a_0, \dots, a_{H_{\text{cut}}}, 0, b_0, \dots, b_{H_{\text{cut}}}, 0)$ as initial values. The code commences with an initial cut-off value of H_{min} , and the optimization procedure is repeated by incrementing H_{cut} until optimization fails. At that point, continued values is computed based on the last converged solution. It is crucial to carefully consider the value assigned to H_{min} , as in certain circumstances, utilizing $H_{\text{min}} = 0$ can fail at the first optimization step. Hence, the optimal value of H_{min} that leads to convergence should be adopted in such cases.

2.3 Hamburger moment problem

The prior knowledge of the moments of the spectral function can be incorporated into the Nevanlinna analytic continuation procedure [46, 59]. The n -th moment is defined as

$$h_n \equiv \int d\omega \omega^n \rho(\omega). \quad (39)$$

These moments are related to the asymptotic expansion of the Green function:

$$G(z) = \int_{-\infty}^{\infty} d\omega \frac{\rho(\omega)}{z - \omega} \quad (40)$$

$$= \frac{1}{z} \int_{-\infty}^{\infty} d\omega \frac{\rho(\omega)}{1 - (\frac{\omega}{z})} \quad (41)$$

$$= \frac{1}{z} \int_{-\infty}^{\infty} d\omega \sum_{n=0}^{\infty} \left(\frac{\omega}{z}\right)^n \rho(\omega) \quad (42)$$

$$= \frac{h_0}{z} + \frac{h_1}{z^2} + \frac{h_2}{z^3} + \dots \quad (|z| \rightarrow \infty). \quad (43)$$

The correct high-frequency data is usually enforced by Matsubara points at large Matsubara frequencies, especially on non-uniform grids with Matsubara points at very high frequencies. However, a cutoff of Matsubara frequencies in the input data, or via the Pick selection criterion, eliminates this information, leading to spectral functions that may have incorrect moments. Imposing constraints on the moments during the interpolation can therefore improve the accuracy of the continued fraction in the Nevanlinna analytic continuation process. The enforcement of moments and the combination of the moment with the interpolation problem is known as the Hamburger Moment Problem [44, 46, 60].

Let us consider a sequence of moments, $b = (h_0, h_1, h_2, \dots, h_{2N-2})$. The vector b is referred to as the Hankel vector and can be pre-calculated by the equations of motion [61, 62]. Our objective is to determine a non-decreasing measure $\sigma(\omega)$ that satisfies the following relationship:

$$h_n = \int_{-\infty}^{\infty} \omega^n d\sigma(\omega). \quad (44)$$

for $n = 0, 1, 2, \dots, 2N-2$. The spectral function is given by $\rho(\omega) = \frac{d\sigma(\omega)}{d\omega}$ (≥ 0). According to the Hamburger-Nevalinna theorem [60], there is a one-to-one correspondence between the class of solutions $\sigma(\omega)$ and a subset of Nevanlinna functions:

$$f(z) = \int_{-\infty}^{\infty} \frac{d\sigma(\omega)}{\omega - z}. \quad (45)$$

This Nevanlinna function has the following asymptotic form:

$$f(z) = -\frac{h_0}{z} - \frac{h_1}{z^2} - \frac{h_2}{z^3} - \dots - \frac{h_{2N-2}}{z^{2N-1}} - o\left(\frac{1}{z^{2N-1}}\right), \quad (46)$$

where the domain of $f(z)$ is $\epsilon < \arg z < \pi - \epsilon$ for some $0 < \epsilon < \frac{\pi}{2}$.

The continuation of $f(z)$ is only possible if the Hankel matrix $H_{NN}[b]$, which is defined as follows:

$$H_{kl}[b] = (h_{i+j})_{i,j=0}^{i=k-1, j=l-1}, \quad k+l = 2N \quad (47)$$

is considered ‘‘proper.’’ The characteristic degrees of the Hankel matrix are defined as $n_1 = \text{rank } H_{NN}[b]$ and $n_2 = 2N - n_1$. A Hankel matrix A is considered proper when its leading submatrix, $B = (A_{i,j})_{i,j=0}^{i=n_1-1, j=n_1-1}$, of order $n_1 \times n_1$ is non-singular, meaning that $n_1 = \text{rank } B$ [63]. Note that a non-singular Hankel matrix is proper.

We introduce a polynomial space defined by the kernel of the Hankel matrix, as given by the following equation:

$$\mathcal{A}_l = (1, z, z^2, \dots, z^{l-1}) \ker(H_{kl}[b]). \quad k + l = 2N \quad (48)$$

In constructing a solution, we utilize two distinct types of polynomials. Let us denote the first type as $p(z)$ and $q(z)$. When $n_1 = n_2 = N$, the dimension of \mathcal{A}_{n_1+1} is 2 and $p(z)$ and $q(z)$ serve as a basis for this space. However, when $n_1 < n_2$, \mathcal{A}_{n_1+1} has a dimension of 1 and $p(z)$ serves as its basis. Meanwhile, the set $p(z), zp(z), \dots, z^{n_2-n_1}p(z), q(z)$ forms an orthogonal basis for \mathcal{A}_{n_2+1} .

The polynomials $p(z)$ and $q(z)$ are not uniquely defined, but a special pair of canonical polynomials is often utilized for convenience. The expression for n_1 -th order polynomial is given by

$$\alpha \det \begin{bmatrix} h_0 & h_1 & \cdots & h_{n_1} \\ h_1 & h_2 & \cdots & h_{n_1+1} \\ \vdots & \vdots & & \vdots \\ h_{n_1-1} & h_{n_1} & \cdots & h_{2n_1-1} \\ 1 & z & \cdots & z^{n_1} \end{bmatrix}, \quad (49)$$

where α is a normalization coefficient that ensures that the polynomial is monic. In the case where $n_1 = N$, h_{2n_1-1} is an arbitrary real number [59]. We choose $p(z)$ to be an n_1 -th order orthogonal polynomial and $q(z)$ to be an $(n_1 - 1)$ -th order polynomial. The polynomials can be expressed as:

$$p(z) = \sum_{n=0}^{n_1} p_n z^n, \quad (50)$$

$$q(z) = \sum_{n=0}^{n_2} q_n z^n. \quad (51)$$

Additionally, we define the symmetrizers of $p(z)$ and $q(z)$ as follows:

$$S(p(z)) = \begin{pmatrix} p_1 & \cdots & p_{n_1-1} & p_{n_1} \\ \vdots & \cdot & \cdot & 0 \\ p_{n_1-1} & \cdot & \cdot & \vdots \\ p_{n_1} & 0 & \cdots & 0 \end{pmatrix}, \quad (52)$$

$$S(q(z)) = \begin{pmatrix} q_1 & \cdots & q_{n_2-1} & q_{n_2} \\ \vdots & \cdot & \cdot & 0 \\ q_{n_2-1} & \cdot & \cdot & \vdots \\ q_{n_2} & 0 & \cdots & 0 \end{pmatrix}. \quad (53)$$

Finally, we introduce the second sets of polynomials, which are the conjugate polynomials of $p(z)$ and $q(z)$:

$$\gamma(z) = (1, z, z^2, \dots, z^{n_1-1}) S(p(z)) (h_0, h_1, \dots, h_{n_1-1})^\top, \quad (54)$$

$$\delta(z) = (1, z, z^2, \dots, z^{n_2-1}) S(q(z)) (h_0, h_1, \dots, h_{n_2-1})^\top. \quad (55)$$

The solutions to the problem are provided for both the case of a positive definite Hankel matrix ($H_{NN} > 0$) and the case of a semi-positive definite Hankel matrix ($H_{NN} \geq 0$), as follows (see Theorem 3.6 in Ref. [59]):

$$f(z) = \int_{-\infty}^{\infty} \frac{d\sigma(\omega)}{\omega - z} \quad (56)$$

$$= \begin{cases} -\frac{\gamma(z) + \varphi(z)\delta(z)}{p(z) + \varphi(z)q(z)} & (H_{NN} > 0), \\ -\frac{\gamma(z)}{p(z)} & (H_{NN} \geq 0 \text{ and proper}). \end{cases} \quad (57)$$

Here, $\varphi(z)$ represents any Nevanlinna function such that $\varphi(z)/z$ approaches zero as $|z|$ approaches infinity.

These frameworks can be combined with the Schur algorithm by incorporating Nevanlinna analytic continuation. Given the data for $f(z)$ to be interpolated,

$$f(Y_\alpha) = \lambda_\alpha \quad (\alpha = 1, 2, \dots, M), \quad (58)$$

we modify data by polynomials $p(z)$, $q(z)$, $\gamma(z)$, $\delta(z)$, as follows:

$$\varphi(Y_\alpha) = \tilde{\lambda}_\alpha = -\frac{\gamma(Y_\alpha) + \lambda_\alpha p(Y_\alpha)}{\delta(Y_\alpha) + \lambda_\alpha q(Y_\alpha)} \quad (\alpha = 1, 2, 3, \dots, M). \quad (59)$$

Since $\varphi(z)$ is a Nevanlinna function, Schur algorithm interpolates the data in Eq. (59) and gives $\varphi(z)$ and $f(z)$.

3 Usage

3.1 Installation

The installation of the library is straightforward by virtue of Julia's package manager. To install, start Julia with the REPL and enter the following in package mode:

```
pkg> add Nevanlinna
```

Then, you are ready to use our library as follows:

```
julia> using Nevanlinna
```

To run the sample code shown below, please install SparseIR.jl additionally as follows:

```
pkg> add SparseIR
```

3.2 Interface

First, arrays containing data for the Matsubara Green function $\mathcal{G}(i\omega_n)$ and the Matsubara frequency $i\omega_n$ are needed. The constructor `NevanlinnaSolver` and `HamburgerNevanlinnaSolver` combined with Nevanlinna analytic continuation can be used for the bare Nevanlinna analytic continuation and the Hamburger moment problem, respectively: For the bare Nevanlinna analytic continuation,

```
julia> sol = NevanlinnaSolver(wn, gw, N_real, w_max, eta, sum_rule,
    H_max, iter_tol, lambda)
```

For the Hamburger moment problem,

```
julia> sol = HamburgerNevanlinnaSolver(moments, wn, gw, N_real, w_max,
    eta, sum_rule, H_max, iter_tol, lambda)
```

In the above code, wn and gw are the array of $i\omega_n$ and $\mathcal{G}(i\omega_n)$, while $moments$ contains the data of moments of $\rho(\omega)$. N_real represents the number of mesh in real axis and w_max represents the energy cutoff of real axis. eta and sum_rule describe the broaden parameter η and $\int d\omega \rho(\omega)$ respectively. H_max , $iter_tol$, and $lambda$ define the upper cut off of H in Hardy optimization, the upper bound of iteration, the regularization parameter in Eq. (38) which are hyperparameters used in calculations. The other parameters are summarized in Table 1. The constructor `HamburgerNevanlinnaSolver` requires an additional input array, `moments`. Within the constructors, the optimal N_{opt} and H_{min} are calculated automatically. The Hardy optimization can then be performed by executing the `solve!` function, as shown below:

```
julia> solve!(sol)
```

Table 1: Arguments of constructors of `NevanlinnaSolver` and `HamburgerNevanlinnaSolver`. The first argument, `moments`, is needed only for `HamburgerNevanlinnaSolver`.

Variable	Type	Description
<code>moments</code>	<code>Vector{Complex{T}}</code>	Array of h_n Only for <code>HamburgerNevanlinnaSolver</code>
<code>wn</code>	<code>Vector{Complex{T}}</code>	Array of $i\omega_n$
<code>gw</code>	<code>Vector{Complex{T}}</code>	Array of $\mathcal{G}(i\omega_n)$
<code>N_real</code>	<code>Int64</code>	The number of mesh in real axis
<code>w_max</code>	<code>Float64</code>	Energy cutoff of real axis
<code>eta</code>	<code>Float64</code>	Broaden parameter η
<code>sum_rule</code>	<code>Float64</code>	$\int d\omega \rho(\omega)$
<code>H_max</code>	<code>Int64</code>	Upper cut off of H
<code>iter_tol</code>	<code>Int64</code>	Upper bound of iteration
<code>lambda</code>	<code>Float64</code>	Regularization parameter λ
<code>verbose</code>	<code>Bool</code>	Verbose option (Default: <code>false</code>)
<code>pick_check</code>	<code>Bool</code>	Causality check option (Default: <code>true</code>)
<code>optimization</code>	<code>Bool</code>	Hardy optimization option (Default: <code>true</code>)
<code>mesh</code>	<code>Symbol</code>	Mesh on real axis option (Default: <code>:linear</code>)

3.3 Example: two-peak model

To illustrate the capabilities of our code, we present a numerical analytic continuation of a two-peak model, which was previously analyzed in Ref. [44]. As shown in Fig. 2, the exact spectral

function is given by the superposition of two Gauss distributions:

$$\rho(\omega) = 0.8 g(\omega, -1.0, 1.0) + 0.2 g(\omega, 3.0, 0.7), \quad (60)$$

where

$$g(\omega, \mu, \sigma) = \frac{1}{\sqrt{2\pi}\sigma} \exp\left\{-\frac{(\omega - \mu)^2}{2\sigma^2}\right\}. \quad (61)$$

We prepare input data $\mathcal{G}(i\omega_n)$ on a sparse sampling Matsubara frequencies, i.e., the intermediate representation grid for $\beta = 100$, generated by using `SparseIR.jl` [64]. The code is shown in Fig. 1. After the analytic continuation is performed, the output data can be accessed through `sol.reals`. The result is shown in Fig. 2. Without Hardy optimization, the continued result shows artificial oscillations around the exact spectral function. However, by the Hardy optimization implemented in our code, these oscillations are effectively removed and the continued spectral function is in good agreement with the exact function.

To demonstrate the significance of using multiple precision arithmetic in the Schur algorithm, we compare the results obtained with 64-bit arithmetic and 128-bit arithmetic. The optimized result is shown in Fig. 3. The result obtained with 64-bit arithmetic is incorrect, as the small peak is not properly restored and there is finite spectral weight in the high- ω region. This indicates that the rounding error in the Schur algorithm can significantly impact the continued result. Hence, it is necessary to use multiple precision arithmetic to guarantee that the rounding error is negligible in the calculation.

In computations at low temperatures, the Matsubara frequencies are close to each other in the complex ω -plane, making it difficult to access high-frequency behavior that may have been truncated by Pick selection. Adding information about the moments can improve the results in these situations. Figure 4 illustrates the influence of the use of moment information on the outcomes. The addition of information leads to a reduction of artificial oscillations. This augmentation stabilizes the numerical computation during Hardy optimization. The Hardy optimization still works efficiently even in the case of the Hamburger moment problem. The inclusion of moments is beneficial in low-temperature calculations or situations where input data is limited.

4 Conclusion

In this paper, we introduced the Julia library `Nevanlinna.jl`. We provided an overview of the analytic structure of Green function, Schur algorithm, Pick criterion, Hardy optimization, and Hamburger moment problem. The Matsubara and retarded Green function on the upper half plane is classified into Nevanlinna function. The Schur algorithm efficiently interpolates and constructs a Nevanlinna function in which the causality can be ensured automatically. The Pick criterion serves as the mathematical base for the existence of Nevanlinna interpolants. We implemented the Hardy optimization using efficient automatic differentiation. The Hamburger moment problem enables analytic continuation with constraints on the moments of a spectral function. We demonstrated the usage of our code, with an example of a two-peak model.

The installation of our code is extraordinarily easy using the Julia package manager. Furthermore, multiple precision arithmetic is already implemented. Thus, there is no obstacle such as building code or installing an external library manually, and users can readily try our code.

Finally, we discuss some remaining technical issues and further extensions to be addressed. In some cases such as Hubbard gap structure, our optimization algorithm of Hardy optimization

```

1  #load package
2  using Nevanlinna
3  using LinearAlgebra
4  using SparseIR
5
6  #set work data Type
7  T = BigFloat
8  setprecision(128)
9
10 #define spectral function
11 gaussian(x, mu, sigma) = exp(-0.5*((x-mu)/sigma)^2)/(sqrt(2*pi)*sigma)
12 rho(omega) = 0.8*gaussian(omega, -1.0, 1.0) + 0.2*gaussian(omega, 3,
13 0.7)
14
15 function generate_input_data(rho::Function, beta::Float64)
16     lambda = 1e+4
17     wmax = lambda/beta
18     basis = FiniteTempBasisSet(beta, wmax, 1e-15)
19
20     rhol = [overlap(basis.basis_f.v[l], rho) for l in 1:length(basis.
21     basis_f)]
22     gl = - basis.basis_f.s .* rhol
23     gw = evaluate(basis.smpl_wn_f, gl)
24
25     hnw = length(basis.smpl_wn_f.sampling_points)÷2
26
27     input_smpl = Array{Complex{T}}(undef, hnw)
28     input_gw = Array{Complex{T}}(undef, hnw)
29     for i in 1:hnw
30         input_smpl[i] = SparseIR.valueim(basis.smpl_wn_f.
31         sampling_points[hnw+i], beta)
32         input_gw[i] = gw[hnw+i]
33     end
34     return input_smpl, input_gw
35 end
36
37 beta = 100. #inverse temperature
38 input_smpl, input_gw = generate_input_data(rho, beta)
39
40 N_real = 1000 #demension of array of output
41 omega_max = 10.0 #energy cutoff of real axis
42 eta = 0.001 #broaden parameter
43 sum_rule = 1.0 #sum rule
44 H_max = 50 #cutoff of Hardy basis
45 lambda = 1e-4 #regularization parameter
46 iter_tol = 1000 #upper bound of iteration
47
48 #construct solver struct
49 sol = NevanlinnaSolver(input_smpl, input_gw, N_real, omega_max, eta,
50     sum_rule, H_max, iter_tol, lambda, verbose=true)
51
52 #execute optimize
53 solve!(sol)

```

Figure 1: Example code for the two-peak model. The results are shown in Fig. 2.

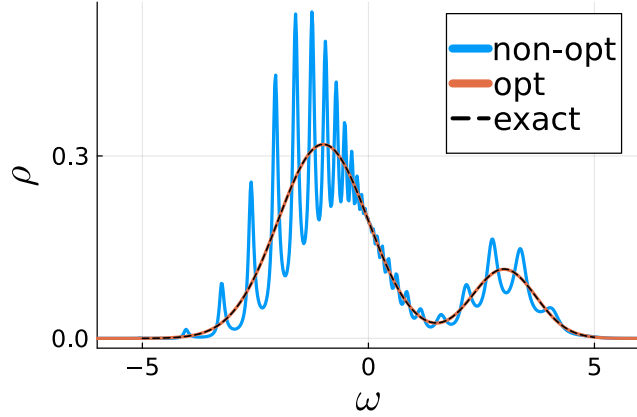


Figure 2: Results of two peak model with and without optimization in Nevanlinna.jl. The exact spectral function consists of two Gaussian peaks [Eq. (60)].

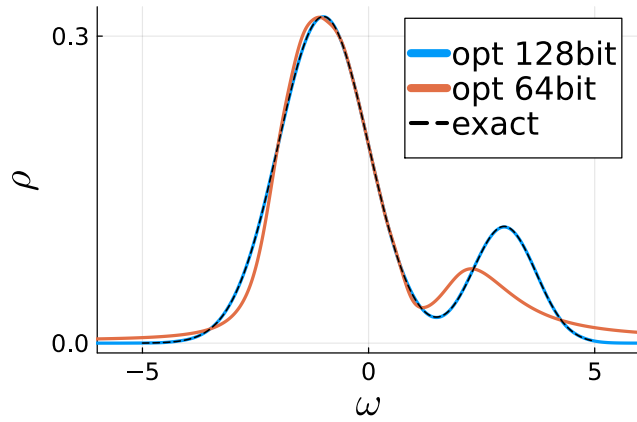


Figure 3: Results of the two-peak model obtained by 64-bit and 128-bit arithmetic. The spectral function is the same as Fig. 2.

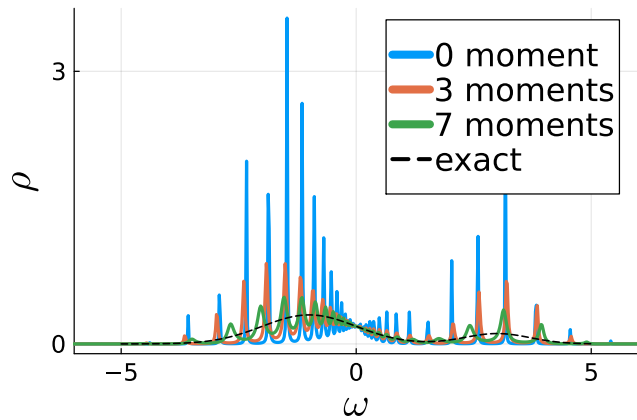


Figure 4: Results of the two-peak model for $\beta = 1000$ and $\eta = 0.0001$. We imposed constraints on the first 0, 3, 7 moments, respectively. The spectral function is the same as Fig. 2.

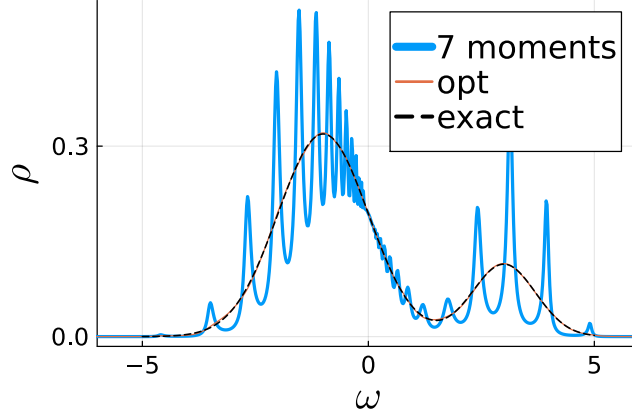


Figure 5: Results with smoothing and constraints on the first 7 moments. The spectral function is the same as Fig. 2.

can not find the optimal solution $\theta_{M+1}(z)$. However, the existence of *true* undetermined function $\theta_{M+1}(z)$ is ensured by Pick criterion, and therefore, further investigation on the optimization algorithm will improve the range of application of Nevanlinna analytic continuation. The extension for the matrix-valued Green function is also an interesting topic. This topic is solved for spectral functions like the δ -function [45], but broadened cases have not been investigated yet. In addition, further expansion of Nevanlinna analytic continuation to self-energy [65] or anomalous Green function [66] is crucial for wide range application of many-body physics.

Acknowledgements

The authors are grateful to T. Koretsune, S. Namerikawa, and F. Kakizawa for fruitful discussions.

Funding information K.N. was supported by JSPS KAKENHI (Grants No. JP21J23007) and Research Grants, 2022 of WISE Program, MEXT. H.S. was supported by JSPS KAKENHI Grants No. 18H01158, No. 21H01041, and No. 21H01003, and JST PRESTO Grant No. JPMJPR2012, Japan. E.G. was supported by the National Science Foundation under Grant No. NSF DMR 2001465.

The code is available under the MIT license at <https://github.com/SpM-lab/Nevalinna.jl>

A Structure of code

A.1 Processing flow

The function `calc_opt_N_imag` calculates the optimal cut-off number `opt_N_imag` to preserve causality as described in Sec. 2.2.3. Then, with the calculated `opt_N_imag`, `calc_phis` calculate ϕ_α as described in Sec. 2.2.4. Next, $a(z)$, $b(z)$, $c(z)$, and $d(z)$ are evaluated on $z = \omega + i\eta$ by `calc_abcd` with Schur algorithm. Finally, optimal `H_min` is evaluated by `calc_H_min` and the Hardy optimization is executed. The flowchart of our procedure is shown in Fig. 6 and the functions in the flowchart are summarized in Table 2.

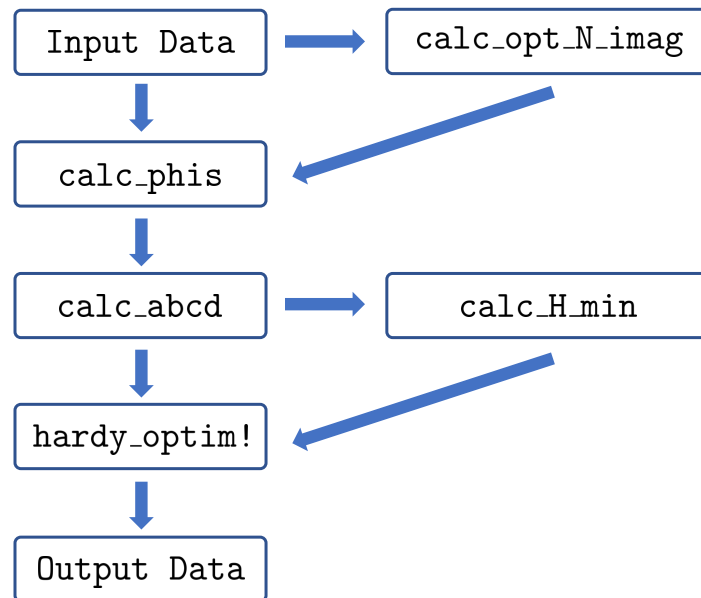


Figure 6: Flowchart of Nevanlinna.jl

Table 2: The functions in processing flow

Variable	Described section
calc_opt_N_imag	Sec. 2.2.3
calc_phis	Sec. 2.2.4
calc_abcd	Sec. 2.2.4
calc_H_min	Sec. 2.2.5

A.2 Data struct

We prepare two struct type which contains input data and output data. In `ImagDomainData`, input data are stored. In Table 3, the member variables of `ImagDomainData` are summarized. `freq` and `val` stores $i\omega_n$ and $h_i(-\mathcal{G}(i\omega_n))$ respectively and `N_imag` represent the dimension of `freq` and `val`. Similarly, in `RealDomainData`, output data are stored. In Table 4, the member variables of `RealDomainData` are summarized. `freq` and `val` stores $\omega + i\eta$ and $-G^R(\omega + i\eta)$ respectively, `N_real` represent the dimension of `freq` and `val`, `omega_max` represent the energy cutoff of real axis, `eta` represent the broaden parameter, and `sum_rule` represent the value of $\int d\omega \rho(\omega)$.

Table 3: The members of `ImagDomainData`

Variable	Type	Description
<code>N_imag</code>	<code>Int64</code>	Dimension of <code>freq</code> and <code>val</code>
<code>freq</code>	<code>Vector{Complex{T}}</code>	$i\omega_n$
<code>val</code>	<code>Vector{Complex{T}}</code>	$h_i(-\mathcal{G}(i\omega_n))$

Table 4: The members of `RealDomainData`

Variable	Type	Description
<code>N_real</code>	<code>Int64</code>	Dimension of <code>freq</code> and <code>val</code>
<code>w_max</code>	<code>Float64</code>	Energy cutoff of real axis
<code>eta</code>	<code>Float64</code>	Broaden parameter η
<code>sum_rule</code>	<code>Float64</code>	$\int d\omega \rho(\omega)$
<code>freq</code>	<code>Vector{Complex{T}}</code>	$\omega + i\eta$
<code>val</code>	<code>Vector{Complex{T}}</code>	$-G^R(\omega + i\eta)$

A.3 Solver struct

We prepare the solver struct of Nevalinna analytic continuation and Hamburger moment problem combined with Nevalinna analytic continuation whose member variables are summarized in Table 5 and Table 6. The constructor executes from `calc_opt_N_imag` to `calc_H_min` in the flowchart in Fig. 6. The function `solve!` executes the Hardy optimization step and `RealDomainData` in the `NevalinnaSolver` has output data.

References

- [1] A. A. Abrikosov, L. P. Gorkov and I. E. Dzyaloshinski, *Methods of quantum field theory in statistical physics*, Courier Corporation (2012).
- [2] A. L. Fetter and J. D. Walecka, *Quantum theory of many-particle systems*, Courier Corporation (2012).
- [3] A. M. Zagoskin, *Quantum theory of many-body systems*, vol. 174, Springer (1998).
- [4] R. D. Mattuck, *A guide to Feynman diagrams in the many-body problem*, Courier Corporation (1992).

Table 5: The members of NevanlinnaSolver

Variable	Type	Description
imags	ImagDomainData{T}	Imaginary domain data
reals	RealDomainData{T}	Real domain data
phis	Vector{Complex{T}}	ϕ_i
abcd	Array{Complex{T}, 3}	$a(z), b(z), c(z)$, and $d(z)$
H_max	Int64	Upper cut off of H
H_min	Int64	Lower cut off of H
H	Int64	Current value of H
ab_coeff	Vector{Complex{T}}	Current solution for a_k, b_k
hardy_matrix	Array{Complex{T}, 2}	Hardy matrix for H
iter_tol	Int64	Upper bound of iteration
lambda	Float64	Regularization parameter
verbose	Bool	Verbose option

Table 6: The members of HamburgerNevanlinnaSolver

Variable	Type	Description
moments	Vector{Complex{T}}	h_n
N_moments_	Int64	Demension of moments
N	Int64	$(N_moments_+1)/2$
n_1	Int64	$\text{rank } H_{NN}[b]$
n_1	Int64	$2N - n_1$
isPSD	Bool	Whether is $H_{NN}[b]$ positive semi definite or not
isProper	Bool	Whether is $H_{NN}[b]$ proper or not
isProper	Bool	Whether is $H_{NN}[b]$ singular or not
isDegenerate	Bool	Whether is $H_{NN}[b]$ degenerate or not
p	Vector{Complex{T}}	p_i
q	Vector{Complex{T}}	q_i
gamma	Vector{Complex{T}}	γ_i
delta	Vector{Complex{T}}	δ_i
hankel	Array{Complex{T}, 2}	Hankel matrix $H_{NN}[b]$
mat_real_omega	Array{Complex{T}, 2}	Matrix of ω^n
val	Vector{Complex{T}}	$f(z)$
nev_st	NevanlinnaSolver{T}	NevanlinnaSolver for $\phi(z)$
verbose	Bool	Verbose option

- [5] G. D. Mahan, *Many-particle physics*, Springer Science & Business Media (2013).
- [6] J. W. Negele, *Quantum many-particle systems*, CRC Press (2018).
- [7] A. Altland and B. D. Simons, *Condensed matter field theory*, Cambridge university press (2010).
- [8] P. W. Anderson, *Absence of diffusion in certain random lattices*, Phys. Rev. **109**, 1492 (1958), doi:[10.1103/PhysRev.109.1492](https://doi.org/10.1103/PhysRev.109.1492).
- [9] P. Nozieres, *Theory of interacting Fermi systems*, CRC Press (2018).
- [10] D. Pines, *Theory of Quantum Liquids: Normal Fermi Liquids*, CRC Press (2018).
- [11] S. Onari, Y. Yamakawa and H. Kontani, *Sign-reversing orbital polarization in the nematic phase of fese due to the C_2 symmetry breaking in the self-energy*, Phys. Rev. Lett. **116**, 227001 (2016), doi:[10.1103/PhysRevLett.116.227001](https://doi.org/10.1103/PhysRevLett.116.227001).
- [12] R. Tazai, S. Matsubara, Y. Yamakawa, S. Onari and H. Kontani, *Rigorous formalism for unconventional symmetry breaking in fermi liquid theory and its application to nematicity in fese*, Phys. Rev. B **107**, 035137 (2023), doi:[10.1103/PhysRevB.107.035137](https://doi.org/10.1103/PhysRevB.107.035137).
- [13] H. Kontani, R. Tazai, Y. Yamakawa and S. Onari, *Unconventional density waves and superconductivities in fe-based superconductors and other strongly correlated electron systems*, Advances in Physics **0**(0), 1 (2023), doi:[10.1080/00018732.2022.2144590](https://doi.org/10.1080/00018732.2022.2144590), <https://doi.org/10.1080/00018732.2022.2144590>.
- [14] T. Moriya and K. Ueda, *Spin fluctuations and high temperature superconductivity*, Advances in Physics **49**(5), 555 (2000), doi:[10.1080/000187300412248](https://doi.org/10.1080/000187300412248), <https://doi.org/10.1080/000187300412248>.
- [15] Y. Yanase, T. Jujo, T. Nomura, H. Ikeda, T. Hotta and K. Yamada, *Theory of superconductivity in strongly correlated electron systems*, Physics Reports **387**(1), 1 (2003), doi:<https://doi.org/10.1016/j.physrep.2003.07.002>.
- [16] A. Georges, G. Kotliar, W. Krauth and M. J. Rozenberg, *Dynamical mean-field theory of strongly correlated fermion systems and the limit of infinite dimensions*, Rev. Mod. Phys. **68**, 13 (1996), doi:[10.1103/RevModPhys.68.13](https://doi.org/10.1103/RevModPhys.68.13).
- [17] J. E. Hirsch and R. M. Fye, *Monte carlo method for magnetic impurities in metals*, Phys. Rev. Lett. **56**, 2521 (1986), doi:[10.1103/PhysRevLett.56.2521](https://doi.org/10.1103/PhysRevLett.56.2521).
- [18] A. N. Rubtsov, V. V. Savkin and A. I. Lichtenstein, *Continuous-time quantum monte carlo method for fermions*, Phys. Rev. B **72**, 035122 (2005), doi:[10.1103/PhysRevB.72.035122](https://doi.org/10.1103/PhysRevB.72.035122).
- [19] P. Werner, A. Comanac, L. de' Medici, M. Troyer and A. J. Millis, *Continuous-time solver for quantum impurity models*, Phys. Rev. Lett. **97**, 076405 (2006), doi:[10.1103/PhysRevLett.97.076405](https://doi.org/10.1103/PhysRevLett.97.076405).
- [20] P. Werner and A. J. Millis, *Hybridization expansion impurity solver: General formulation and application to kondo lattice and two-orbital models*, Phys. Rev. B **74**, 155107 (2006), doi:[10.1103/PhysRevB.74.155107](https://doi.org/10.1103/PhysRevB.74.155107).

- [21] E. Gull, A. J. Millis, A. I. Lichtenstein, A. N. Rubtsov, M. Troyer and P. Werner, *Continuous-time monte carlo methods for quantum impurity models*, Rev. Mod. Phys. **83**, 349 (2011), doi:[10.1103/RevModPhys.83.349](https://doi.org/10.1103/RevModPhys.83.349).
- [22] T. DeGrand and C. DeTar, *Lattice Methods for Quantum Chromodynamics*, WORLD SCIENTIFIC, doi:[10.1142/6065](https://doi.org/10.1142/6065) (2006), <https://www.worldscientific.com/doi/pdf/10.1142/6065>.
- [23] C. Gattringer and C. Lang, *Quantum chromodynamics on the lattice: an introductory presentation*, vol. 788, Springer Science & Business Media (2009).
- [24] H. J. Rothe, *Lattice Gauge Theories : An Introduction (Fourth Edition)*, vol. 43, World Scientific Publishing Company, ISBN 978-981-4365-87-1, 978-981-4365-85-7, doi:[10.1142/8229](https://doi.org/10.1142/8229) (2012).
- [25] A. Filinov, *Correlation effects and collective excitations in bosonic bilayers: Role of quantum statistics, superfluidity, and the dimerization transition*, Phys. Rev. A **94**, 013603 (2016), doi:[10.1103/PhysRevA.94.013603](https://doi.org/10.1103/PhysRevA.94.013603).
- [26] K. Nogaki and H. Shinaoka, *Bosonic nevanlinna analytic continuation*, Journal of the Physical Society of Japan **92**(3), 035001 (2023), doi:[10.7566/JPSJ.92.035001](https://doi.org/10.7566/JPSJ.92.035001).
- [27] M. Boninsegni and D. M. Ceperley, *Density fluctuations in liquid ^4He . path integrals and maximum entropy*, Journal of Low Temperature Physics **104**(5), 339 (1996), doi:[10.1007/BF00751861](https://doi.org/10.1007/BF00751861).
- [28] E. Vitali, M. Rossi, L. Reatto and D. E. Galli, *Ab initio low-energy dynamics of superfluid and solid ^4He* , Phys. Rev. B **82**, 174510 (2010), doi:[10.1103/PhysRevB.82.174510](https://doi.org/10.1103/PhysRevB.82.174510).
- [29] S. Sacconi, S. Moroni and M. Boninsegni, *Excitation spectrum of a supersolid*, Phys. Rev. Lett. **108**, 175301 (2012), doi:[10.1103/PhysRevLett.108.175301](https://doi.org/10.1103/PhysRevLett.108.175301).
- [30] T. Dornheim, S. Groth, J. Vorberger and M. Bonitz, *Ab initio path integral monte carlo results for the dynamic structure factor of correlated electrons: From the electron liquid to warm dense matter*, Phys. Rev. Lett. **121**, 255001 (2018), doi:[10.1103/PhysRevLett.121.255001](https://doi.org/10.1103/PhysRevLett.121.255001).
- [31] G. A. Baker, G. A. Baker Jr, P. Graves-Morris and S. S. Baker, *Pade Approximants: Encyclopedia of Mathematics and It's Applications, Vol. 59 George A. Baker, Jr., Peter Graves-Morris*, vol. 59, Cambridge University Press (1996).
- [32] R. K. Bryan, *Maximum entropy analysis of oversampled data problems*, European Biophysics Journal **18**(3), 165 (1990), doi:[10.1007/BF02427376](https://doi.org/10.1007/BF02427376).
- [33] M. Jarrell and J. Gubernatis, *Bayesian inference and the analytic continuation of imaginary-time quantum monte carlo data*, Physics Reports **269**(3), 133 (1996), doi:[https://doi.org/10.1016/0370-1573\(95\)00074-7](https://doi.org/10.1016/0370-1573(95)00074-7).
- [34] A. W. Sandvik, *Stochastic method for analytic continuation of quantum monte carlo data*, Phys. Rev. B **57**, 10287 (1998), doi:[10.1103/PhysRevB.57.10287](https://doi.org/10.1103/PhysRevB.57.10287).
- [35] A. S. Mishchenko, N. V. Prokof'ev, A. Sakamoto and B. V. Svistunov, *Diagrammatic quantum monte carlo study of the fröhlich polaron*, Phys. Rev. B **62**, 6317 (2000), doi:[10.1103/PhysRevB.62.6317](https://doi.org/10.1103/PhysRevB.62.6317).

- [36] K. Vafayi and O. Gunnarsson, *Analytical continuation of spectral data from imaginary time axis to real frequency axis using statistical sampling*, Phys. Rev. B **76**, 035115 (2007), doi:[10.1103/PhysRevB.76.035115](https://doi.org/10.1103/PhysRevB.76.035115).
- [37] S. Fuchs, M. Jarrell and T. Pruschke, *Application of bayesian inference to stochastic analytic continuation*, Journal of Physics: Conference Series **200**(1), 012041 (2010), doi:[10.1088/1742-6596/200/1/012041](https://doi.org/10.1088/1742-6596/200/1/012041).
- [38] O. Goulko, A. S. Mishchenko, L. Pollet, N. Prokof'ev and B. Svistunov, *Numerical analytic continuation: Answers to well-posed questions*, Phys. Rev. B **95**, 014102 (2017), doi:[10.1103/PhysRevB.95.014102](https://doi.org/10.1103/PhysRevB.95.014102).
- [39] H. Yoon, J.-H. Sim and M. J. Han, *Analytic continuation via domain knowledge free machine learning*, Phys. Rev. B **98**, 245101 (2018), doi:[10.1103/PhysRevB.98.245101](https://doi.org/10.1103/PhysRevB.98.245101).
- [40] J. Otsuki, M. Ohzeki, H. Shinaoka and K. Yoshimi, *Sparse modeling approach to analytical continuation of imaginary-time quantum monte carlo data*, Phys. Rev. E **95**, 061302 (2017), doi:[10.1103/PhysRevE.95.061302](https://doi.org/10.1103/PhysRevE.95.061302).
- [41] J. Otsuki, M. Ohzeki, H. Shinaoka and K. Yoshimi, *Sparse modeling in quantum many-body problems*, Journal of the Physical Society of Japan **89**(1), 012001 (2020), doi:[10.7566/JPSJ.89.012001](https://doi.org/10.7566/JPSJ.89.012001).
- [42] L. Ying, *Analytic continuation from limited noisy matsubara data*, Journal of Computational Physics **469**, 111549 (2022), doi:[10.1016/j.jcp.2022.111549](https://doi.org/10.1016/j.jcp.2022.111549).
- [43] Z. Huang, E. Gull and L. Lin, *Robust analytic continuation of green's functions via projection, pole estimation, and semidefinite relaxation*, doi:[10.48550/ARXIV.2210.04187](https://doi.org/10.48550/ARXIV.2210.04187) (2022).
- [44] J. Fei, C.-N. Yeh and E. Gull, *Nevanlinna analytical continuation*, Phys. Rev. Lett. **126**, 056402 (2021), doi:[10.1103/PhysRevLett.126.056402](https://doi.org/10.1103/PhysRevLett.126.056402).
- [45] J. Fei, C.-N. Yeh, D. Zgid and E. Gull, *Analytical continuation of matrix-valued functions: Carathéodory formalism*, Phys. Rev. B **104**, 165111 (2021), doi:[10.1103/PhysRevB.104.165111](https://doi.org/10.1103/PhysRevB.104.165111).
- [46] J. Fei, *A probe into propagators*, <https://dx.doi.org/10.7302/1312>, doi:[10.7302/1312](https://doi.org/10.7302/1312) (2021).
- [47] T. Matsubara, *A New Approach to Quantum-Statistical Mechanics*, Progress of Theoretical Physics **14**(4), 351 (1955), doi:[10.1143/PTP.14.351](https://doi.org/10.1143/PTP.14.351).
- [48] H. Umezawa and S. Kamefuchi, *The Vacuum in Quantum Electrodynamics*, Progress of Theoretical Physics **6**(4), 543 (1951), doi:[10.1143/ptp/6.4.543](https://doi.org/10.1143/ptp/6.4.543).
- [49] G. Källén, *On the definition of the renormalization constants in quantum electrodynamics*, Helvetica Physica Acta **25**(IV), 417 (1952), doi:[10.5169/seals-112316](https://doi.org/10.5169/seals-112316).
- [50] M. Gell-Mann and F. E. Low, *Quantum electrodynamics at small distances*, Phys. Rev. **95**, 1300 (1954), doi:[10.1103/PhysRev.95.1300](https://doi.org/10.1103/PhysRev.95.1300).

- [51] H. Lehmann, *Über eigenschaften von ausbreitungsfunktionen und renormierungskonstanten quantisierter felder*, Il Nuovo Cimento (1943-1954) **11**(4), 342 (1954), doi:[10.1007/BF02783624](https://doi.org/10.1007/BF02783624).
- [52] J. Schur, *Über potenzreihen, die im innern des einheitskreises beschränkt sind.*, Journal für die reine und angewandte Mathematik (Crelles Journal) **1918**(148), 122 (1918), doi:[doi:10.1515/crll.1918.148.122](https://doi.org/10.1515/crll.1918.148.122).
- [53] V. M. Adamyan, J. Alcober and I. M. Tkachenko, *Reconstruction of distributions by their moments and local constraints*, Applied Mathematics Research eXpress **2003**(2), 33 (2003), doi:[10.1155/S1687120003212028](https://doi.org/10.1155/S1687120003212028), <https://academic.oup.com/amrx/article-pdf/2003/2/33/6920279/2003-2-33.pdf>.
- [54] G. Pick, *Über die beschränkungen analytischer funktionen durch vorgegebene funktionswerte*, Mathematische Annalen **78**(1), 270 (1917), doi:[10.1007/BF01457103](https://doi.org/10.1007/BF01457103).
- [55] P. Khargonekar and A. Tannenbaum, *Non-euclidian metrics and the robust stabilization of systems with parameter uncertainty*, IEEE Transactions on Automatic Control **30**(10), 1005 (1985), doi:[10.1109/TAC.1985.1103805](https://doi.org/10.1109/TAC.1985.1103805).
- [56] M. Rosenblum and J. Rovnyak, *Topics in Hardy classes and univalent functions*, Springer Science & Business Media (1994).
- [57] M. Innes, *Don't unroll adjoint: Differentiating ssa-form programs*, CoRR **abs/1810.07951** (2018), [1810.07951](https://arxiv.org/abs/1810.07951).
- [58] P. K. Mogensen and A. N. Riseth, *Optim: A mathematical optimization package for Julia*, Journal of Open Source Software **3**(24), 615 (2018), doi:[10.21105/joss.00615](https://doi.org/10.21105/joss.00615).
- [59] G. ning Chen, *The general rational interpolation problem and its connection with the nevanlinna-pick interpolation and power moment problem*, Linear Algebra and its Applications **273**(1), 83 (1998), doi:[https://doi.org/10.1016/S0024-3795\(97\)00346-7](https://doi.org/10.1016/S0024-3795(97)00346-7).
- [60] N. I. Akhiezer, *The Classical Moment Problem and Some Related Questions in Analysis*, Society for Industrial and Applied Mathematics, Philadelphia, PA, doi:[10.1137/1.9781611976397](https://doi.org/10.1137/1.9781611976397) (2020), <https://epubs.siam.org/doi/pdf/10.1137/1.9781611976397>.
- [61] A.-B. Comanac, *Dynamical mean field theory of correlated electron systems: New algorithms and applications to local observables*, Ph.D. thesis, Columbia University, New York (2007).
- [62] E. Gull, *Continuous-Time Quantum Monte Carlo Algorithms for Fermions*, Doctoral thesis, ETH Zurich, Zürich, doi:[10.3929/ethz-a-005722583](https://doi.org/10.3929/ethz-a-005722583) (2008).
- [63] M. Fiedler, *Quasidirect decompositions of hankel and toeplitz matrices*, Linear Algebra and its Applications **61**, 155 (1984), doi:[https://doi.org/10.1016/0024-3795\(84\)90028-4](https://doi.org/10.1016/0024-3795(84)90028-4).
- [64] M. Wallerberger, S. Badr, S. Hoshino, S. Huber, F. Kakizawa, T. Koretsune, Y. Nagai, K. Nogaki, T. Nomoto, H. Mori, J. Otsuki, S. Ozaki *et al.*, *sparse-ir: Optimal compression and sparse sampling of many-body propagators*, SoftwareX **21**, 101266 (2023), doi:<https://doi.org/10.1016/j.softx.2022.101266>.

- [65] X. Wang, E. Gull, L. de' Medici, M. Capone and A. J. Millis, *Antiferromagnetism and the gap of a mott insulator: Results from analytic continuation of the self-energy*, Phys. Rev. B **80**, 045101 (2009), doi:[10.1103/PhysRevB.80.045101](https://doi.org/10.1103/PhysRevB.80.045101).
- [66] E. Gull and A. J. Millis, *Quasiparticle properties of the superconducting state of the two-dimensional hubbard model*, Phys. Rev. B **91**, 085116 (2015), doi:[10.1103/PhysRevB.91.085116](https://doi.org/10.1103/PhysRevB.91.085116).